Noise studies with Crab Cavities in the SPS for the HL-LHC project

Thesis submitted in accordance with the requirements of the University of Liverpool for the degree of Doctor in Philosophy

by

Natalia Triantafyllou

Day Month Year

Abstract

Acknowledgments

List of Figures

List of Tables

List of Symbols

E_b	Energy
f_{rev}	Revolution frequency
V_{RF}	Main RF voltage
f_{RF}	Main RF frequency
CC	Crab Cavity
V_{CC}	CC voltage
f_{CC}	CC frequency
ϕ_{CC}	CC phase
β_{CC}	Beta function at the CC
Q_x	Horizontal tune
Q_y	Vertical tune
$\mathrm{Q_s}$	Synchrotron tune
D_x	Horizontal dispersion function
D_y	Vertical dispersion function
β	Relativistic beta
γ	Relativistic gamma (Lorenz factor)
N_b	Bunch intensity i.e. number of particles (here protons)
Q'_x	Horizontal first order chromaticity
Q'_y	Vertical first order chromaticity

Contents

1 | Introduction

This is the introduction of my PhD thesis.

1. General about standard model (Sofia, Schenk) 2. Role of CERN 3. Role of my thesis.

1.1 The CERN accelerator complex

1.2 Crab Cavities for High-Luminosity LHC

1.3 Project objectives and thesis outline

1.4 General parameters of the studies

The studies presented in this thesis were performed for the nominal SPS optics for the LHC filling which are called Q26 optics as the higher integer part of the tune in both planes is 26. These optics can be found in the official CERN repository [1] and will be referred to as the SPS model in this thesis. The values of the optics parameters in what follows correspond to the model values unless stated otherwise.

Probably put to abstract In 2018, two prototype Crab Cavities (CCs) were installed in the SPS to be tested for the first time with proton beams. A series of dedicated machine developemnt studies was carried out in order to validate their working principle and answer various beam dynamic questions. One of the operational issues that needed to be addressed concerned the expected emittance growth due to noise in their RF system, which is the main subject this thesis. As mentioned in chapter 3 a theoretical model had already been developed and validated by trackig simulations [2]. As a part of the first experiemental campaign with CCs in SPS a dedicated experiment was conducted to benchmark these models with experimental data and confirm the analytical predictions. The objective of this chapter is to provide an overview of the machine setup for the CC experiements and introduce the instruments and methods used for measuring the beam parameters of interest for the emittance growth studies.

2 | Basics of accelerator beam dynamics

For a gaussian beam distribution the normalised beam emittance is defined as:

$$\epsilon_x = \frac{\sigma_x(s)^2 - \delta^2 D_x^2(s)}{\beta_x(s)} \beta\gamma \tag{2.1}$$

where $\sigma_x(s)$ is the beam size, $\beta_x(s)$ is the beta function, $D_x(s)$ is the dispersion fat a specific location s along the accelerator, $\delta = \Delta p / p0$ is the momentum spread and β, γ the relativistic parameters. Similar expression is valid for the vertical plane, with the difference that there is no dispersion.

Standard deviation

The standard deviation (SD) is a measure of the spread of a set of values. It is defined as follows:

$$\sigma = \sqrt{\frac{\sum (x_i - \mu)^2}{N}}, \tag{2.2}$$

where σ is the standard deviation N is the size of the set, x_i each value of the set and μ the mean of the set.

3 | Theory of Crab Cavity noise induced emittance growth

For a uniform noise spectrum across the betatron tune distribution, the emittance growth resulting from amplitude noise can be estimated from:

$$\frac{d\epsilon}{dt} = \beta_{CC}\left(\frac{eV_{CC}f_{rev}}{2E_b}\right)^2 C_{\Delta A}(\sigma_\phi)\sum_{k=-\infty}^{+\infty} S_{\Delta A}[(k\pm\bar{\nu}_b\pm\bar{\nu}_s)f_{rev}]. \tag{3.1}$$

For phase noise, the emittance growth can be estimated from:

$$\frac{d\epsilon}{dt} = \beta_{CC}\left(\frac{eV_{CC}f_{rev}}{2E_b}\right)^2 C_{\Delta\phi}(\sigma_\phi)\sum_{k=-\infty}^{+\infty} S_{\Delta\phi}[(k\pm\bar{\nu}_b)f_{rev}]. \tag{3.2}$$

In these formulae, β_{CC} is the beta function at the location of the CC, V_{CC} the CC voltage, f_{rev} the revolution frequency of the beam, E_b the beam energy, and $\bar{\nu}_b$ and $\bar{\nu}_s$ the mean of the betatron and synchrotron tune distribution. $S_{\Delta A}$ and $S_{\Delta\phi}$ are the power spectral densities (PSD) [3] of the noise at all the betatron and synchrobetatron (for the amplitude noise case) sidebands. $C_{\Delta A}$ and $C_{\Delta\phi}$ are correction terms to account for the bunch length:

$$C_{\Delta A}(\sigma_\phi) = e^{-\sigma_\phi^2}\sum_{l=0}^{+\infty} I_{2l+1}(\sigma_\phi^2), \tag{3.3}$$

$$C_{\Delta\phi}(\sigma_\phi) = e^{-\sigma_\phi^2}\left[I_0(\sigma_\phi^2) + 2\sum_{l=1}^{+\infty} I_{2l}(\sigma_\phi^2)\right], \tag{3.4}$$

with σ_ϕ the rms bunch length (in radians) with respect to the CC frequency f_{CC}, and $I_n(x)$ the modified Bessel function of the first kind.

4 Calibration of the Crab Cavities for the SPS tests in 2018

In 2018 the CC technology was tested with proton beams in the SPS for the first time. In this chapter, the setup and the calibration of the CCs in the SPS are presented along with the demonstration of the first crabbings of proton beams. The objective is to provide a full understanding of the operational aspects of the CCs in the SPS and the measurement of the CC voltage which is one of the most crucial parameters for the emittance growth studies (see Chapter 3, Eq. (3.1) and Eq. (3.2)).

The chapter is structured as follows: Section 4.1 describes the installation of the CC system in the SPS.

4.1 Crab Cavities installation in the SPS

For the SPS tests two prototype CCs of the Double Quarter Wave (DQW) type , which will be reffered to as CC1 and CC2 throught this thesis, were fabricated by CERN and were assembled in the same cryomodule, shown in Fig. 5.1 [4]. For its installation an available space was found at the SPS Long Straight Section 6 (SPS-LSS6) zone. As this section is also used for the extraction of the beam to the LHC, the cryomodule was placed on a mobile transfer table [5] which moved the cryomodule in the beam-line for the CC tests and out of it for the usual SPS operation without breaking the vaccum.

The main CCs parameters are listed in Table 4.1. Their location along the SPS ring is also indicated, in case someone would like to repeat the analysis described in this thesis.

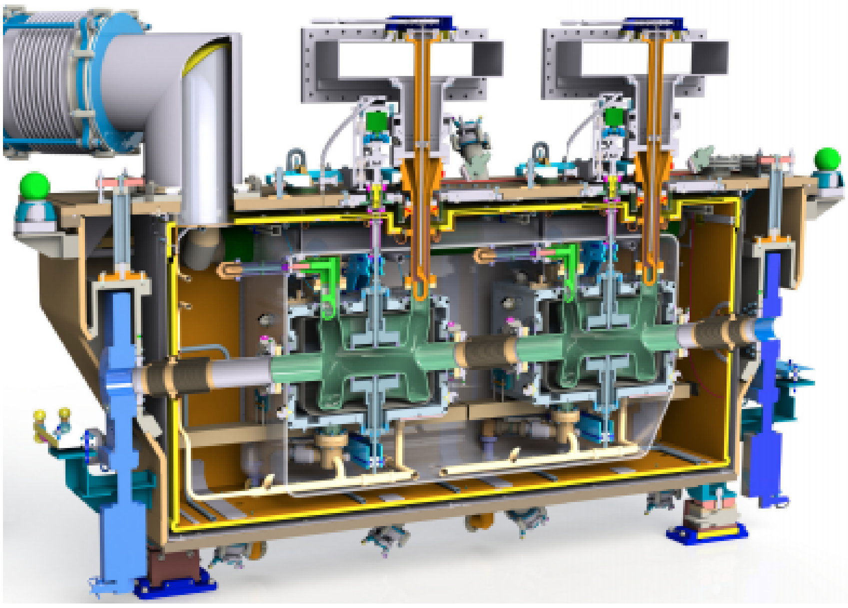

Figure 4.1: Cross section view of the CC cryomodule [4]. It has a total length of 3 m [6] and at its core there are the two DQW cavities, which are illustrated with light green color.

Table 4.1: Crab Cavities design parameters for the SPS tests in 2018.

Parameter	**Value**	
	CC1	**CC2**
crabbing plane	vertical	vertical
s-location*	6312.72 m	6313.32 m
CC voltage, V_{CC}	≤ 3.4 MV	≤ 3.4 MV
CC frequency, f_{CC}	400.78 MHz	400.78 MHz
Horizontal / Vertical beta function, $\beta_{x,CC}$ / $\beta_{y,CC}$	29.24 m / 76.07 m	30.31 m / 73.82 m
Horizontal / Vertical alpha function, $\alpha_{x,CC}$ / $\alpha_{y,CC}$	-0.88 m / 1.9 m	-0.91 m / 1.86 m
Horizontal / Vertical dispersion, $D_{x,CC}$ / $D_{y,CC}$	-0.48 m / 0 m	-0.5 m / 0 m

* The s-location is reffered to the location of the elements along the SPS ring with respect to the start of the lattice i.e. element QF.10010 which is a focusing quadrupole.

4.2 Operational considerations

For the beam tests with CCs in the SPS the approach regarding the energy ramp and the adjustment of the phasing with the main RF system needed to be evaluated and they are briefly discussed here.

Energy ramp

SPS recieves the proton beam at 26 GeV from the PS. It was found that the ramp to higher energies could not be performed with the CC on, as the beam was getting lost while crossing one of the vertical betatron sidebands due to resonant excitation [7]. Therefore, it was established that the acceleration has to be performed with the CC off and its voltage must be set up only after the energy of interest has been achieved. It is worth noting that this approach will also be used in the HL-LHC.

Crab Cavity - main SPS RF synchronisation

It was important to ensure that during the "coast" the beam will epxeriene the same kick from the CC each turn. In other words the SPS main RF system operating at 200 MHz needed to be synchronous with the CC operating at 400 MHz. Due to the larger bandwidth of the SPS main RF system the CC was used as a master. Therefore the CC was operating at a fixed frequency and phase, while the main accelerating cavities were adjusted to the exact half of the CC frequency and were re-phased so that they become synchronous with the crabbing signal. For the studies at higher energies the synchronisation took place at the end of the ramp shortly after the cavity was switched on [8].

4.3 SPS Head-Tail monitor as the main diagnostic

The SPS is equipped with a high bandwidth pick-up of approximately 2 GHz allowing to resolve the intra-bunch motion. This instrument is called Head-Tail (HT) monitor and was originally designed for measuring chromaticity and transverse isntabilities. However, in the SPS CC tests, the HT monitor was the main diagnostic device deployed for the demonstration of the crabbing and the measurement of the CC voltage (explained in details in Section 4.4). Therefore its use as a crabbing diagnostic should be explained here. The methods and procedures described in this section were developed at CERN and they are described here for the completness of the thesis.

In the first part of this section some general information on the instrument along with example signals will be presented. Subsequently, the post processing of the HT signal in the presence of the CC will be discussed. Last, the calibration of the CC voltage from the HT data is described and the visualisation of the crabbing is displayed. The experimental data presented in this section were acquired at the SPS injection energy of 26 GeV with only one CC, CC1, at phase $\phi_{CC} = 0$ for simplicity. That energy of 26 GeV was chosen to provide a better understanding of the methods used as the orbit shift from the CC kick is stronger and thus more visible than in higher energies.

General information

As already mentioned, the HT monitor is a high bandwidth version of a standard beam position monitor, which means that it can measure the transverse displacement within the bunch. This makes it ideal for the measurement of the intra-bunch offset caused from the CC kick. Its reading consists of the sum (Σ) and the difference (Δ) of the electrode signals of a straight stripline coupler (Fig. 5.2) [9, 10] over a defined acquisition period. The sum signal is the longitudinal line density while the difference signal corresponds to the intra-bunch offset. The system operates at time scale where the signals are given as a function of the position within the bunch.

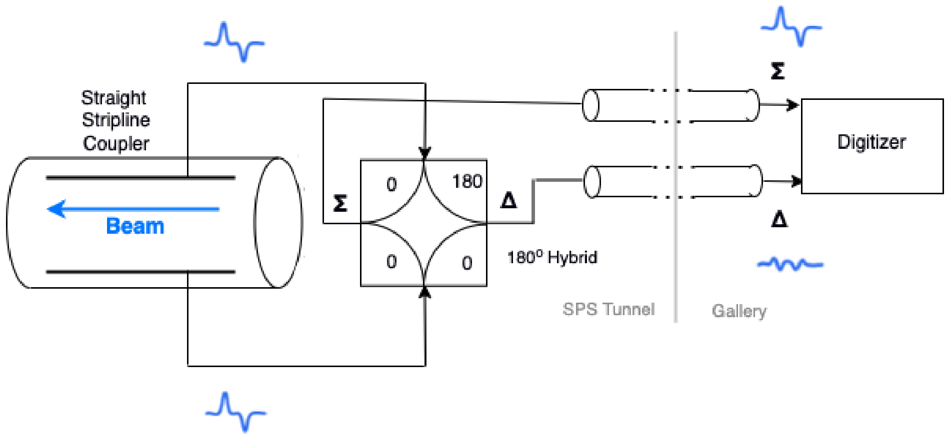

Figure 4.2: Diagram of the SPS HT monitor [10]. The beam is passing through a straight stripline coupler which is followed by a 180°hybrid. This configuration provides the sum (Σ) and the difference (Δ) signal of the two electrodes.

The raw signals from the HT monitor require a specific post-processing procedure, which is described in Ref. [10], in order to give useful information. Figure 5.3 shows some example signals obtained from the HT monitor after the basic post-processing is applied. Moreover, Fig. 5.4 shows a 2D representation of the HT monitor reading. It is worth noting here that in the specific example a clear modulating pattern in time of the vertical intra-bunch offset (vertical Δ) signal is observed. This is a result of the phase slip between the CC and the main RF system because they are not yet synchronised.

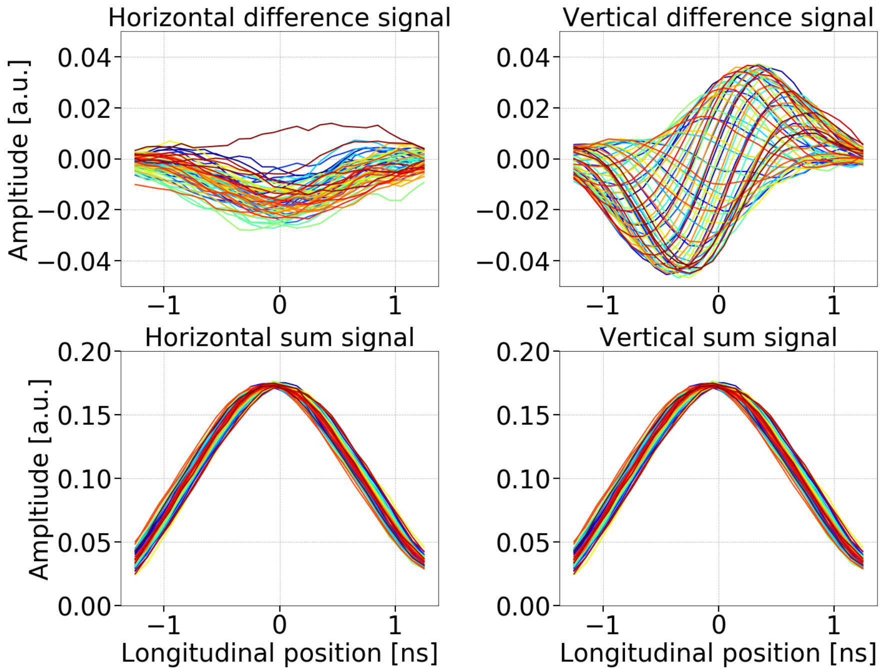

Figure 4.3: Example difference and sum signals (top and bottom plots, respectively) from the HT monitor, in time scale, with respect to the longitudinal position within the bunch over several SPS revolutions, after the basic post processing (Ref. [10]) but before the baseline correction. The different colors indicate the signals from different turns (every 100 turns).

4.3.1 Post processing in the presence of Crab Cavities

To obtain useful information from the HT monitor signal in the presence of the CCs there are a few steps that differ from the standard post processing procedure and they are desribed below.

Head-Tail monitor baseline correction

The HT monitor measurement has a baseline on the difference signal which needs to be removed. The baseline is a result of orbit offsets and non-linearities of the

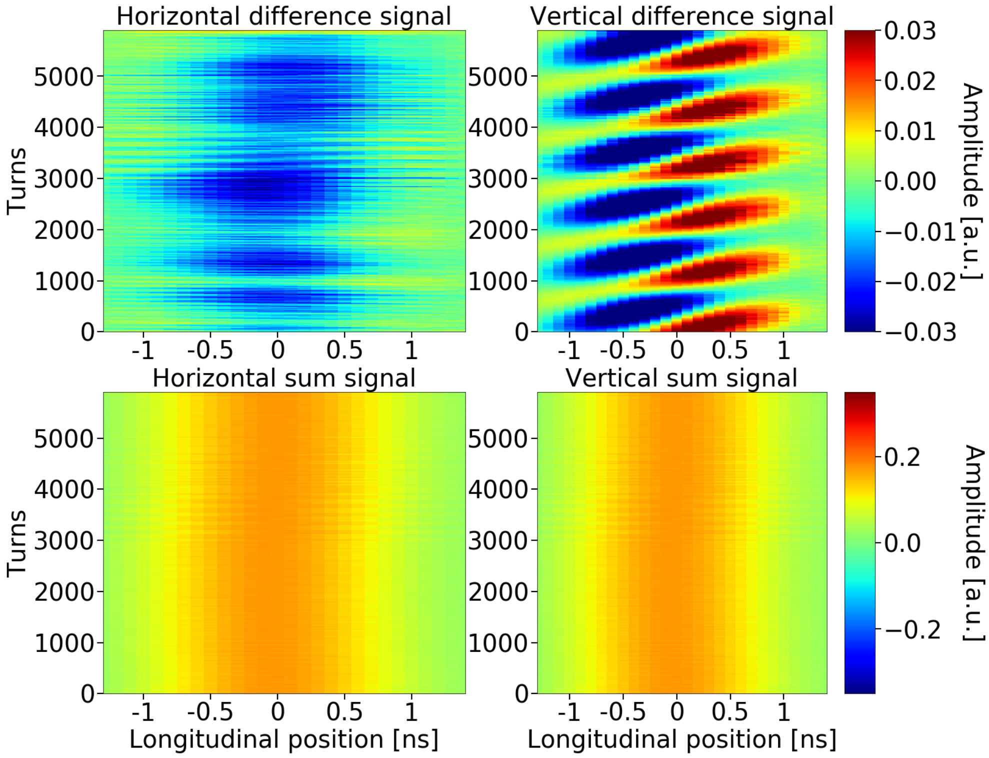

Figure 4.4: 2D representation of example difference and sum signals with respect to the longitudinal position within the bunch obtained from the HT monitor over several SPS revolutions.

instrument and is constant from turn to turn [10]. Therefore, during the normal post processing procedure (without CCs), the baseline is computed as the mean of the difference signals over all turns and then the correction is achieved by subtracting this static offset from the signal of each turn. However, in the SPS tests, where the CCs are well synchronised with the main RF system (Section 5.2), the crabbing signal is also a static intra-bunch position offset and thus would also be removed with the usual method. Because of technical limitations it was not feasible to switch off the CC for those kind of measurements. Thus, the following technique was used.

For the CC experiments a reference measurement had first to be made with the CC not being synchronous with the main RF system. The baseline was computed as the mean of the difference signals over this reference period and subsequently it was subtracted from the average of the difference signals acquired after the synchronisation (Fig 5.5). The datasets before and after synchronisation are easily distinguishable in the 2D HT monitor reading as displayed in Fig. 5.6

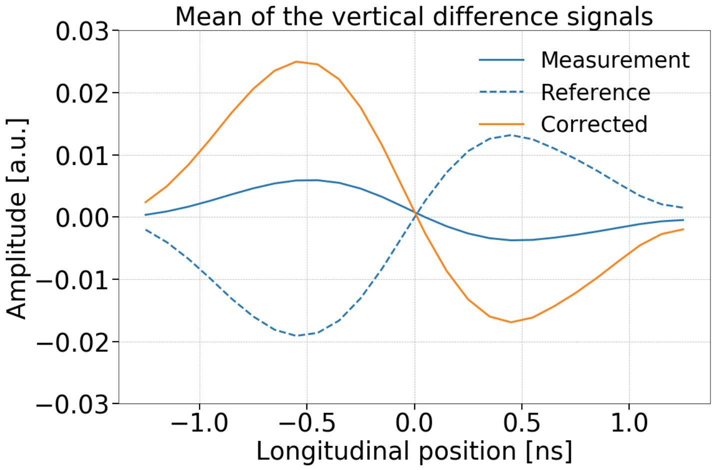

Figure 4.5: HT monitor baseline correction for the SPS CC tests. The baseline signal (blue dashed line) refers to the mean of the difference signals acquired before the CC - main RF synchronisation. The measured signal (blue solid line) corresponds to the mean of the difference signal acquired after the synchronisation. Last, the corrected signal (orange solid line) is obtained after subtracting the baselin from the measured signal.

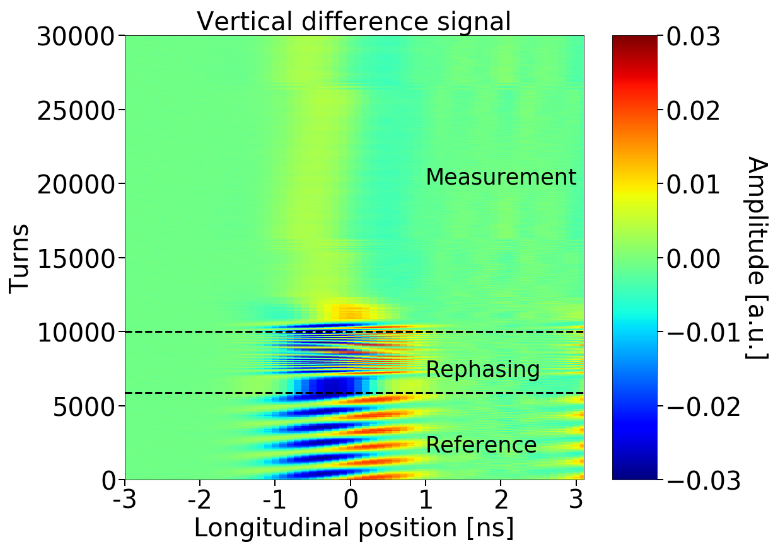

Figure 4.6: HT acquistions before and after the synchronisation of the SPS main RF with the CC.

Head-Tail monitor scaling to millimeters

The last step to make the HT acquisitions meaningful is to convert the measured intra bunch offset, mean of the difference signals after the CC - main RF synchronisation and after the baseline correction, from arbitrary units to millimeters. The scaling is achieved by division with the mean of the sum signals after the synchronisation and with a normalisation factor which is provided by the calibration of the HT monitor [11]. The normalisation factor for the SPS was measured at 0.1052 in 2018 [12]. Figure 5.7 shows the intra-bunch offset from the CC kick in millimeters and after the baseline correction.

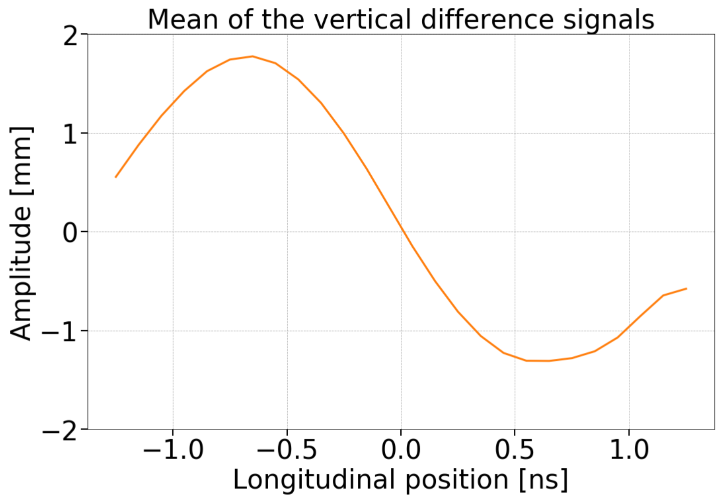

Figure 4.7: Intra-bunch offset from the CC kick expressed in millimeters after the removal of the baseline.

4.3.2 Crab Cavity voltage calibration

This section discusses the beam based measurement of the CC voltage from the HT monitor signal. The calibration was performed by using Eq. (5.1) to calculate the kick required to reconstruct the measured intra-bunch offset. Equation (5.1), which is obtained from Eq. (1) from chapter 4.7.1 in Ref. [13], gives the vertical orbit shift (in meters) from the CC kick, θ, at the HT monitor location as follows:

$$\Delta y_{,HT} = \frac{\sqrt{\beta_{y,HT}}}{2\sin(\pi Q_y)} \theta \sqrt{\beta_{y,CC}} \cos(\pi Q_y - \mid \psi_{y,HT} - \psi_{y,CC} \mid), \tag{4.1}$$

where β_y is the beta function, Q_y is the tune, and $\mid \psi_{y,HT} - \psi_{y,CC} \mid$ between the CC and the HT monitor in tune units. The same applies for the horizontal plane. The subscripts HT and CC indicate quanities at the location of the HT monitor and CC respectively.

The deflection from the CC is written as $\theta = -\frac{qV(t)}{E_b}$, where q is the charge of the particle, E_b the beam energy and $V_{CC}(t) = V_{CC}\sin(2\pi f_{CC} t + \phi_{CC})$ is the voltage that a particle experiences while passing through the CC. In the context where the HT monitor measures the signal as a function of time, t, the voltage in the above formula is expressed accordingly as $V_{CC}(t)$, where $t = 0$ the center of the bunch.

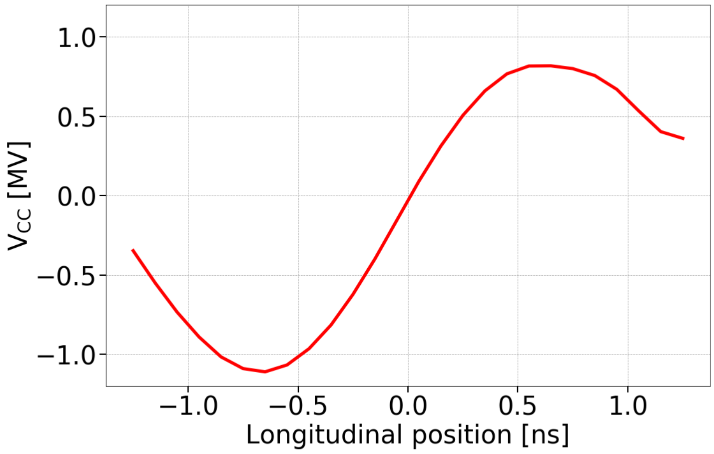

Figure 4.8: CC voltage calibration from the HT monitor.

It should be noted here, that the measured intra-bunch offset, $\Delta y_{,HT}$, is inserted in Eq. (5.1) after removing the baseline and converting it to millimeters as discussed in Section 5.3.1. Figure 5.8 illustrates the cavity voltage computed from the HT signals shown already in this section. The corresponding beam and optic parameters are listed in Table 5.2.

Table 4.2: Parameters for computing the CC voltage from the example HT monitor measurements discussed in this chapter.

Parameter	**Value**
Beta function at the HT monitor, $\beta_{y,HT}$	49.19 m
Phase advance between the start* of the lattice and the HT monitor, $\psi_{y,HT}$	$15.68 \times 2\pi$
Beta function at the CC1, $\beta_{y,CC1}$	76.07 m
Phase advance between the start* of the lattice and CC1, $\psi_{y,CC1}$	$23.9 \times 2\pi$
Vertical betatron tune, Q_y	26.13
Beam energy, E_b	26 GeV

* The start of the lattice is considered the element QF.10010 which is a focusing quadrupole.

Estimation of the amplitude and the uncertainty of the measurement

It is clear from Fig. 5.8 that the reconstructed CC voltage, $V_{CC}(t)$, is not centered around zero. This voltage offset is not a systematic error as it is not in the same direction and has a different value for each measurement. In this case, the amplitude of the signal is defined as half the peak to peak amplitude, $V_{CC} = V_{CC,p-p}/2$. Note that the peak to peak amplitude, $V_{CC,p-p}$, is the difference between the maximum positive and negative peaks of the signal. The uncertainty in the amplitude is defined as the offset that needs to be added or subtracted to the signal, such as it is centered around zero. In other words, the uncertainty, ΔV_{CC}, is defined as half the sum of the maximum positive and negative peaks of the signal. Figure 5.9 shows the peak to peak amplitude, $V_{CC,p-p}$, the amplitude of the signal, V_{CC}, and the uncertainty, ΔV_{CC}, for the reconstructed CC voltage, $V_{CC}(t)$.

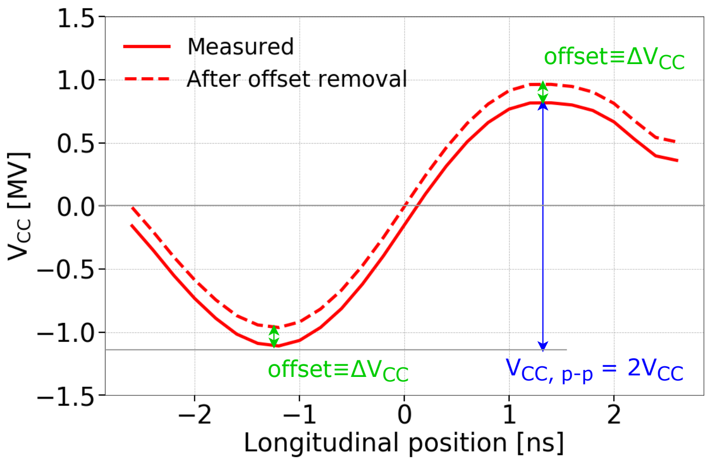

Figure 4.9: Illustration of the CC amplitude voltage, V_{CC}, defined as half the peak to peak amplitude, $V_{CC,p-p}$ (blue) and of its uncertainty, ΔV_{CC}, defined as the offset needed for the signal to be zero-centered. Here, V_{CC}=0.96 MV and ΔV_{CC}=0.15 MV.

Reconstruction of crabbing

Additionally, the measurements from the HT monitor were used for reconstructing the crabbing and representating schematically the beam projection in the transverse plane. The technique for reconstructing the crabbing was developed at CERN in 2018 and was extensively used throught the experimental campaign with CCs since (together with the calibrated voltage) it gives a straightforward estimate of the applied CC kick, as illustrated in Fig. 5.10.

To obtain this schematic representation, which is practically a density plot, of the effect of the CC kick on the beam one needs to multiply the measured longitudinal profile, mean of the sum signals acquired after the synchronisation, with the measured intra-bunch offset, mean of the differene signals acquired after the synchronisation. An example of this is shown in Fig. 5.7. For the transverse plane a gaussian distribution is considered with σ obtained from the wire scanner (addressed in more detail in the following section). The color code of Fig. 5.10 is normalised to the maximum intensity within the bunch.

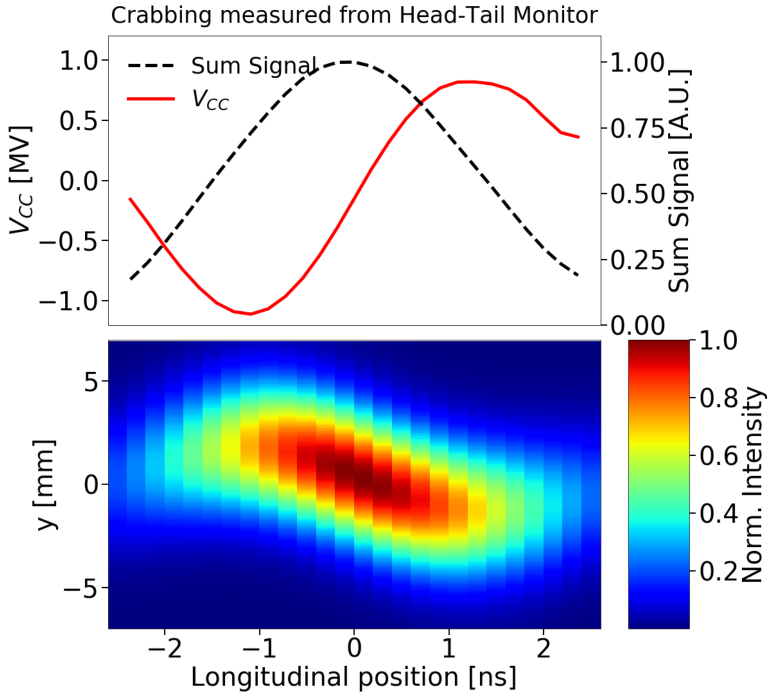

Figure 4.10: Illustration of the crabbing from the HT monitor signal. CC voltage and sum signal (longitudinal line density) measured from the HT monitor (top) together with the density plot (bottom) which visualises the effect of the CC kick in the beam.

4.4 Characterisation of measured Crab Cavity voltage

4.4.1 Dependence of the crab cavity voltage and offset on the phase

Dependence studies Phase scan

5 Experimental studies 2018: Operational setup and beam instrumentation

The theoretical model for the transverse emittance growth caused by amplitude and phase noise in a CC was introduced in Chapter 3. On September 5, 2018, a dedicated experiment was conducted in the SPS to benchmark this model against experimental data and confirm the analytical predictions. In this chapter, the machine setup, the beam configuration and the instrumentation used for the emittance growth studies with CCs in the SPS are presented.

The chapter is structured as follows: Section 5.1 describes the experimental machine configuration. Thereafter, Section 5.2 elaborates on the installation and the operational aspects of the CCs in the SPS. In Sections 5.3- 5.5 the instruments used for the parameters of interest (see Chapter 3, Eq. (3.1) and Eq. (3.2)) i.e. CC voltage, emittance and bunch length are discussed, including the post processing methods where it was performed by the author. The results of the experiment are presented separately in Chapter 6.

5.1 Machine and beam configuration

For studying the long-term emittance evolution a special mode of operation was set up in the SPS which is called "coast" (in other machines, it is referred to as storage ring mode) with bunched beams. In this mode, the bunches circulate in the machine at constant energy for long periods, from a few minutes up to several hours, similar to the HL-LHC case.

To make sure that the SPS can be used as a testbed for the emittance growth studies with CCs an extensive preparatory campaign was carried out through 2012-2017 [14, 15, 16]. The primary concern was the emittance growth that was observed in the machine from other sources than injected noise and will be referred to as the natural emittance growth in this thesis. The natural emittance growth needs to be well characterized and be kept sufficiently small in order to distinguish and understand the contribution from the CC noise. From these studies, it was concluded that the optimal coast setup is at high energies, with low chromaticity and bunches of low intensity as it minimises the natural emittance growth [16]. The highest energy for which the SPS could operate in "coast" was 270 GeV and thus the experiments were performed at this energy. That limitation was introduced due to the rms power deposited in its magnets when operating at high energy for long period of time. Moreover, as the natural emittance growth was found to be a single bunch effect four bunches were used. That choice was made to reduce the statistical uncertainty of the measurements but not to increase the beam intensity.

During the experiment the Landau octupoles were switched off. Nevetherless, a residual non-linearity was present in the machine mainly due to multipole components in the dipole magnets [17, 18]. Last, the transverse feedback system was switched off. The main machine and beam parameters used in the experiment of 2018 are listed in Table 5.1. It should be noted, that no measurements of chromaticity are available from the day of the experiment. However it was ensured that the chromaticity was corrected to small positive values.

5.2 Crab Cavities in the SPS

For the SPS tests two prototype CCs of the Double Quarter Wave (DQW) type, CC1 and CC2, were fabricated by CERN and were assembled in the same cryomodule, shown in Fig. 5.1 [4]. For its istallation For its installation an available space was found at the SPS Long Straight Section 6 (SPS-LSS6) zone. As this section is also used for the extraction of the beam to the LHC, the cryomodule was placed on a mobile transfer table [5] which moved the cryomodule in the beamline for the CC tests and out of it for the usual SPS operation without breaking the vaccum. For the noise induced emittance growth studies only CC2 was used. Nevertheless, the parameters

Table 5.1: Main machine and beam parameters for the emittance growth studies with CCs in SPS in 2018.

Parameter	Value
Beam energy, E_b	270 GeV
Revolution frequency, f_{rev}	43.375 kHz
Number of proton per bunch, N_b	3×10^{10} p/b
Number of bunches	4
Bunch spacing	524 ns
Main RF frequency, f_{RF}	200.39 MHz
Main RF voltage, V_{RF}	3.8 MV
Horizontal / Vertical betatron tune, Q_x / Q_y	26.13 / 26.18
Horizontal / Vertical first order chromaticity, Q'_x / Q'_y	~ 1.0 / ~ 1.0
Synchrotron tune, $\mathrm{Q_s}$	0.0051

for both CCs are shown in Table 4.1 for completeness. In case someone wants to repeat the study, the location of the CCs along the SPS ring is also indicated.

5.2.1 Operational considerations

For the beam tests with the CC in the SPS the approach regarding the energy ramp and the adjustment of the phasing with the main RF system needed to be evaluated and they are briefly discussed here.

Energy ramp

SPS recieves the proton beam at 26 GeV from the PS. It was found that the ramp to higher energies could not be performed with the CC on, as the beam was getting lost while crossing one of the vertical betatron sidebands due to resonant excitation [7]. Therefore, it was established that the acceleration has to be performed with the CC off and its voltage must be set up only after the energy of interest has been achieved. It is worth noting that this approach will also be used in the HL-LHC.

Crab Cavity - main RF synchronisation

It was important to ensure that during the "coast" the beam will epxeriene the same

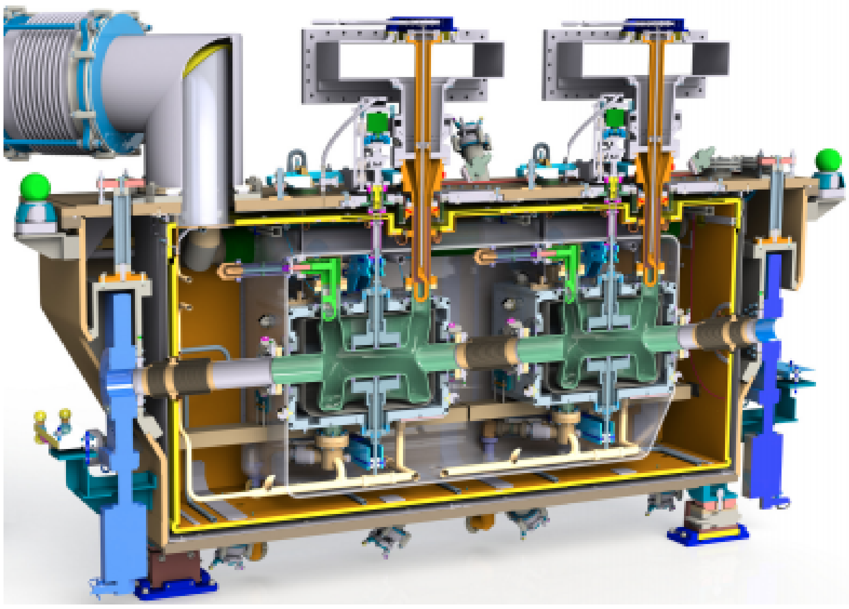

Figure 5.1: Cross section view of the CC cryomodule [4]. It has a total length of 3 m [6] and at its core there are the two DQW cavities, which are illustrated with light green color.

kick from the CC each turn. In other words the SPS main RF system operating at 200 MHz needed to be synchronous with the CC operating at 400 MHz. Due to the larger bandwidth of the SPS main RF system the CC was used as a master. Therefore the CC was operating at a fixed frequency and phase, while the main accelerating cavities were adjusted to the exact half of the CC frequency (see values at Tables 5.1 and 4.1) and were re-phased so that they become synchronous with the crabbing signal. For the studies at 270 GeV the synchronisation took place at the end of the ramp to the coast energy and shortly after the cavity was switched on [8].

5.3 SPS Head-Tail monitor

The SPS is equipped with a high bandwidth pick-up of approximately 2 GHz allowing to resolve the intra-bunch motion. This instrument is called Head-Tail (HT) monitor and was originally designed for measuring chromaticity and transverse isntabilities. However, in the SPS CC tests, the HT monitor was the main diagnostic device deployed for the measurement of the crabbing and the calibration of the CC voltage. Therefore its use as a crabbing diagnostic should be explained here. The methods and procedures described in this section were developed at CERN and they are described here for the completness of the thesis.

In the first part of this section some general information on the instrument along with example signals will be presented. Subsequently, the post processing of the HT signal in the presence of the CC will be discussed. Last, the calibration of the CC voltage from the HT data is described. The experimental data presented in this section were acquired at the SPS injection energy of 26 GeV with only one CC, CC1, at phase $\phi_{CC} = 0$ for simplicity. That energy of 26 GeV was chosen to provide a better understanding of the methods used as the orbit shift from the CC kick is stronger and thus more visible than in higher energies.

General information

As already mentioned, the HT monitor is a high bandwidth version of a standard beam position monitor, which means that it can measure the transverse displacement within the bunch. This makes it ideal for the measurement of the intra-bunch offset caused from the CC kick. Its reading consists of the sum (Σ) and the difference (Δ) of the electrode signals of a straight stripline coupler (Fig. 5.2) [9, 10] over a defined acquisition period. The sum signal is the longitudinal line density while the difference signal corresponds to the intra-bunch offset. The system operates at time scale where the signals are given as a function of the position within the bunch.

The raw signals from the HT monitor require a specific post-processing procedure, which is described in Ref. [10], in order to give useful information. Figure 5.3 shows some example signals obtained from the HT monitor after the basic post-processing is applied. Moreover, Fig. 5.4 shows a 2D representation of the HT monitor reading. It is worth noting here that in the specific example a clear modulating pattern in time of the vertical intra-bunch offset (vertical Δ) signal is observed. This is a result of the phase slip between the CC and the main RF system because they are not yet synchronised.

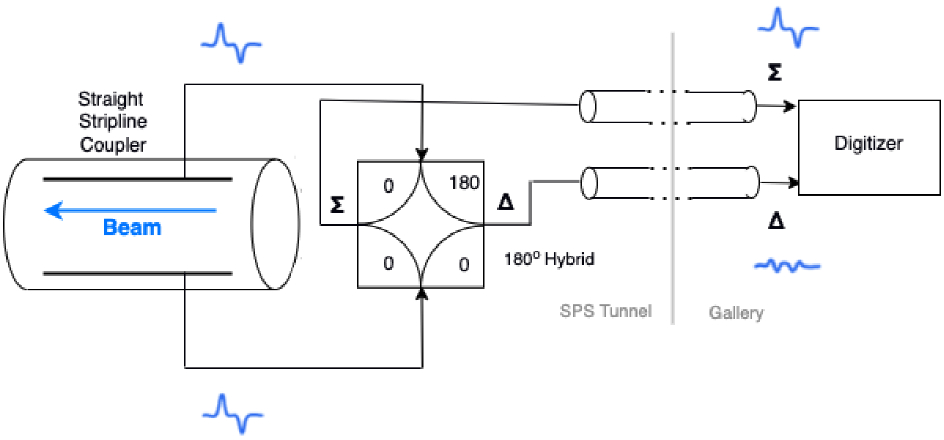

Figure 5.2: Diagram of the SPS HT monitor [10]. The beam is passing through a straight stripline coupler which is followed by a 180°hybrid. This configuration provides the sum (Σ) and the difference (Δ) signal of the two electrodes.

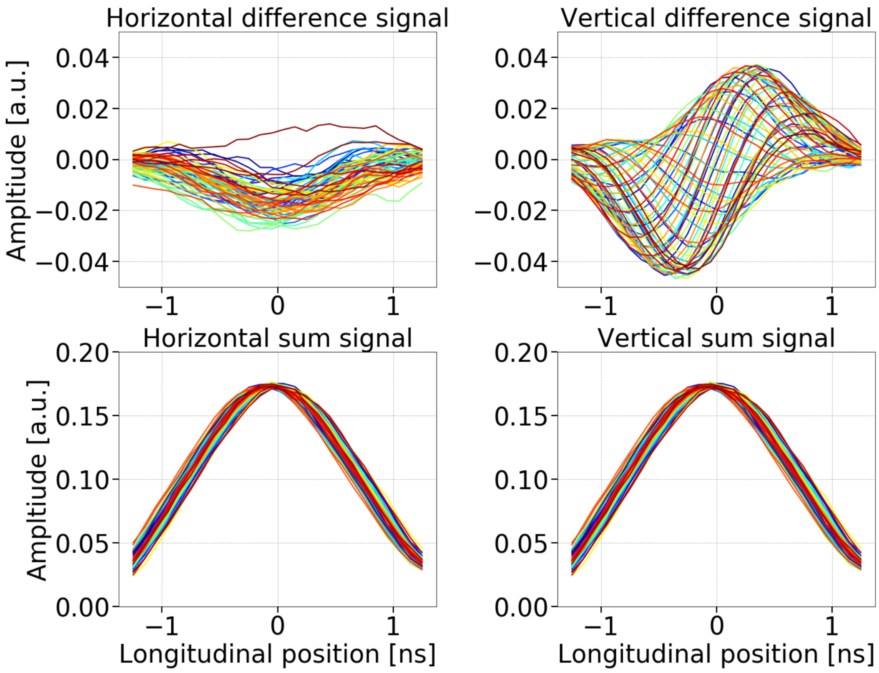

Figure 5.3: Example difference and sum signals (top and bottom plots, respectively) from the HT monitor, in time scale, with respect to the longitudinal position within the bunch over several SPS revolutions, after the basic post processing (Ref. [10]) but before the baseline correction. The different colors indicate the signals from different turns (every 100 turns).

5.3.1 Post processing in the presence of Crab Cavities

To obtain useful information from the HT monitor signal in the presence of the CCs there are a few steps that differ from the standard post processing procedure and

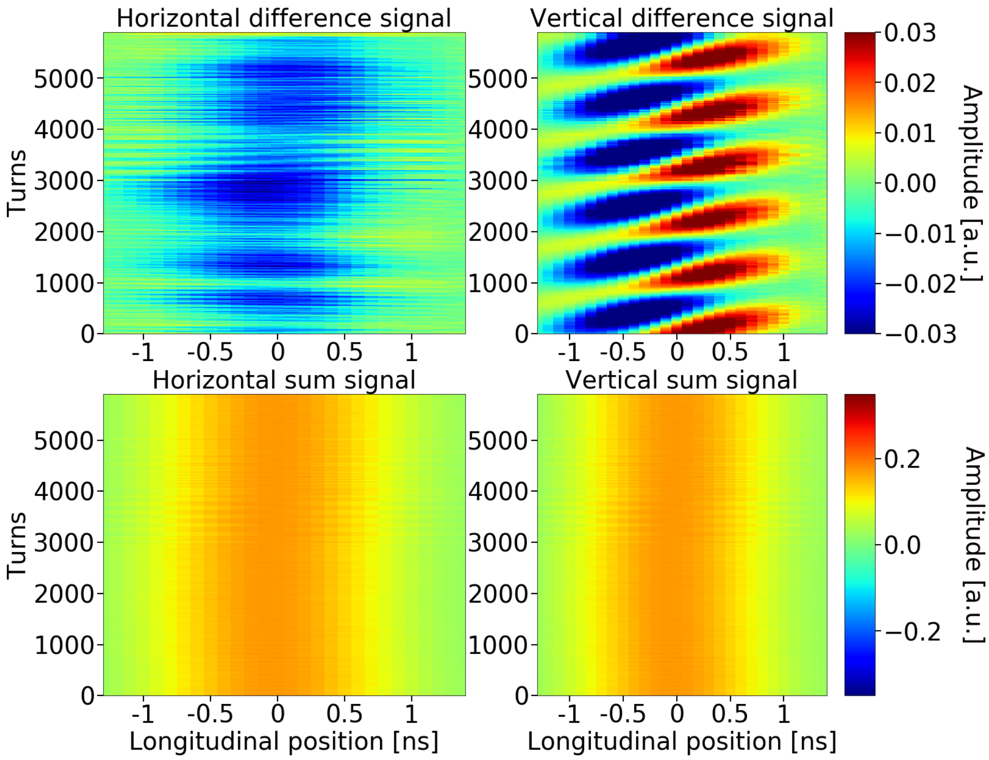

Figure 5.4: 2D representation of example difference and sum signals with respect to the longitudinal position within the bunch obtained from the HT monitor over several SPS revolutions.

they are desribed below.

Head-Tail monitor baseline correction

The HT monitor measurement has a baseline on the difference signal which needs to be removed. The baseline is a result of orbit offsets and non-linearities of the instrument and is constant from turn to turn [10]. Therefore, during the normal post processing procedure (without CCs), the baseline is computed as the mean of the difference signals over all turns and then the correction is achieved by subtracting this static offset from the signal of each turn. However, in the SPS tests, where the CCs are well synchronised with the main RF system (Section 5.2), the crabbing signal is also a static intra-bunch position offset and thus would also be removed with the usual method. Because of technical limitations it was not feasible to switch off the CC for those kind of measurements. Thus, the following technique was used.

For the CC experiments a reference measurement had first to be made with the CC not being synchronous with the main RF system. The baseline was computed as the mean of the difference signals over this reference period and subsequently it was subtracted from the average of the difference signals acquired after the synchronisation (Fig 5.5). The datasets before and after synchronisation are easily distinguishable in the 2D HT monitor reading as displayed in Fig. 5.6

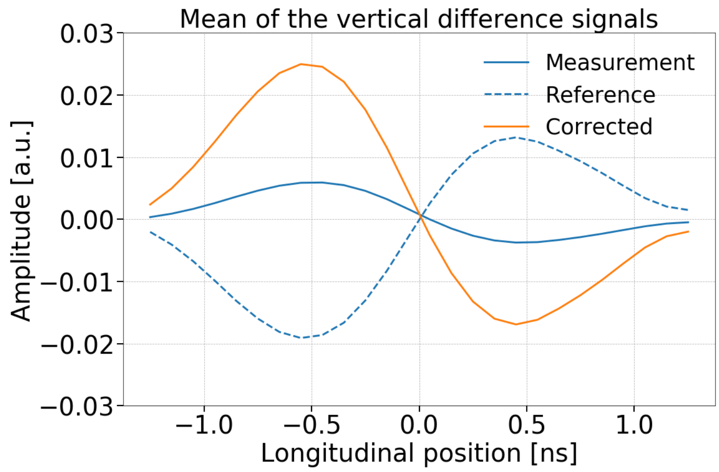

Figure 5.5: HT monitor baseline correction for the SPS CC tests. The baseline signal (blue dashed line) refers to the mean of the difference signals acquired before the CC - main RF synchronisation. The measured signal (blue solid line) corresponds to the mean of the difference signal acquired after the synchronisation. Last, the corrected signal (orange solid line) is obtained after subtracting the baselin from the measured signal.

Head-Tail monitor callibration

The last step to make the HT acquisitions meaningful is to convert the measured intra bunch offset, mean of the difference signals after the CC - main RF synchronisation and after the baseline correction, from arbitrary units to millimeters. The scaling is achieved by division with the mean of the sum signals after the synchronisation and with a normalisation factor which is provided by the calibration of the HT monitor [11]. The normalisation factor for the SPS was measured at 0.1052 in 2018 [12]. Figure 5.7 shows the intra-bunch offset from the CC kick in millimeters and after the baseline correction.

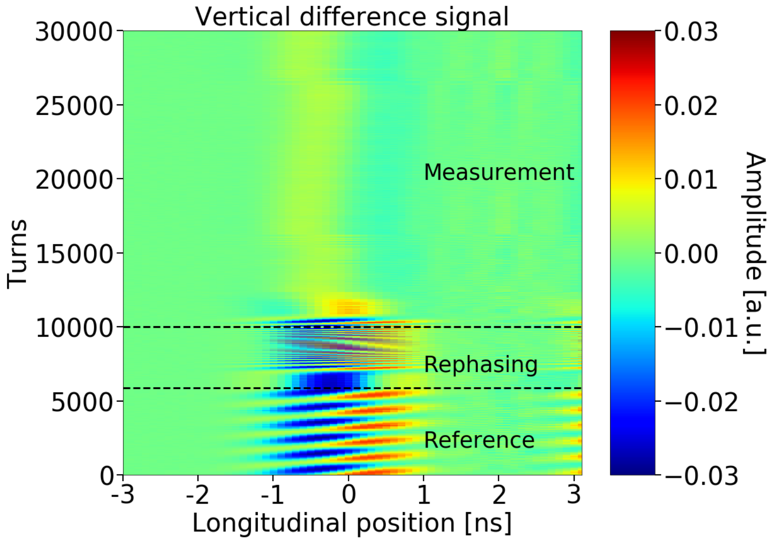

Figure 5.6: HT acquistions before and after the synchronisation of the SPS main RF with the CC.

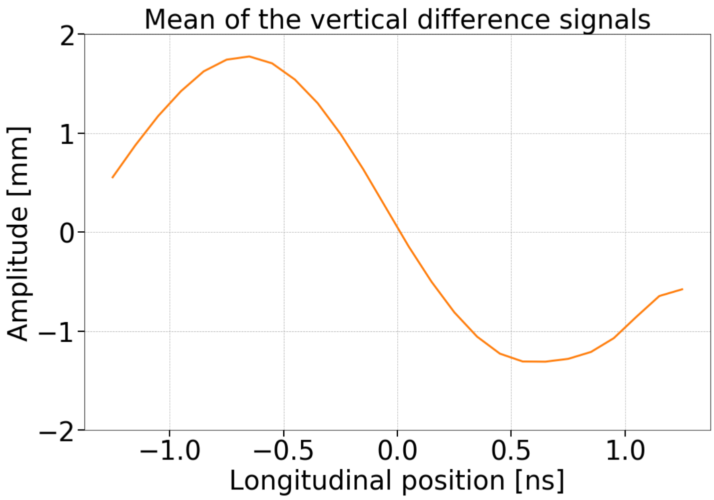

Figure 5.7: Intra-bunch offset from the CC kick expressed in millimeters after the removal of the baseline.

5.3.2 Crab Cavity voltage calibration

This section discusses the beam based measurement of the CC voltage from the HT monitor signal. The calibration was performed by using Eq. (5.1) to calculate the kick required to reconstruct the measured intra-bunch offset. Equation (5.1), which is obtained from Eq. (1) from chapter 4.7.1 in Ref. [13], gives the vertical orbit shift (in meters) from the CC kick, θ, at the HT monitor location as follows:

$$\Delta y_{,HT} = \frac{\sqrt{\beta_{y,HT}}}{2\sin(\pi Q_y)}\theta\sqrt{\beta_{y,CC}}\cos(\pi Q_y - \mid \psi_{y,HT} - \psi_{y,CC} \mid), \tag{5.1}$$

where β_y is the beta function, Q_y is the tune, and $\mid \psi_{y,HT} - \psi_{y,CC} \mid$ between the CC and the HT monitor in tune units. The same applies for the horizontal plane. The subscripts HT and CC indicate quanities at the location of the HT monitor and CC respectively.

The deflection from the CC is written as $\theta = -\frac{qV(t)}{E_b}$, where q is the charge of the particle, E_b the beam energy and $V_{CC}(t) = V_{CC}\sin(2\pi f_{CC}t + \phi_{CC})$ is the voltage that a particle experiences while passing through the CC. In the context where the HT monitor measures the signal as a function of time, t, the voltage in the above formula is expressed accordingly as $V_{CC}(t)$, where $t = 0$ the center of the bunch.

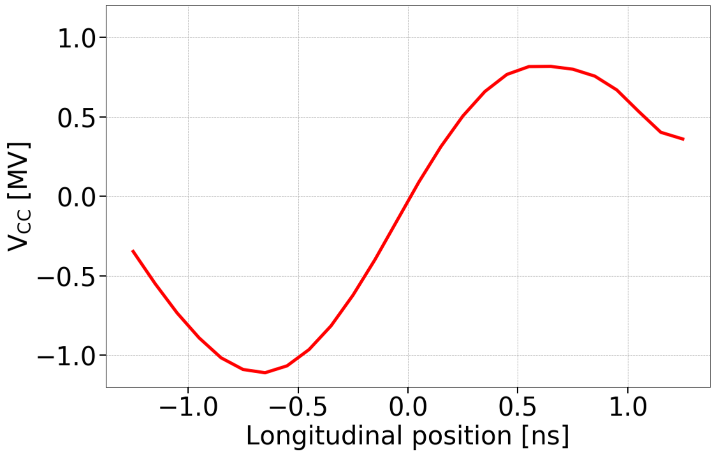

Figure 5.8: CC voltage calibration from the HT monitor.

It should be noted here, that the measured intra-bunch offset, $\Delta y_{,HT}$, is inserted in Eq. (5.1) after removing the baseline and converting it to millimeters as discussed in Section 5.3.1. Figure 5.8 illustrates the cavity voltage computed from the HT signals shown already in this section. The corresponding beam and optic parameters are listed in Table 5.2.

Estimation of the amplitude and the uncertainty of the measurement

It is clear from Fig. 5.8 that the reconstructed CC voltage, $V_{CC}(t)$, is not centered around zero. This voltage offset is not a systematic error as it is not in the same direction and has a different value for each measurement. In this case, the amplitude of the signal is defined as half the peak to peak amplitude, $V_{CC} = V_{CC,p-p}/2$. Note

Table 5.2: Parameters for computing the CC voltage from the example HT monitor measurements discussed in this chapter.

Parameter	**Value**
Beta function at the HT monitor, $\beta_{y,HT}$	49.19 m
Phase advance between the start* of the lattice and the HT monitor, $\psi_{y,HT}$	$15.68 \times 2\pi$
Beta function at the CC1, $\beta_{y,CC1}$	76.07 m
Phase advance between the start* of the lattice and CC1, $\psi_{y,CC1}$	$23.9 \times 2\pi$
Vertical betatron tune, Q_y	26.13
Beam energy, E_b	26 GeV

* The start of the lattice is considered the element QF.10010 which is a focusing quadrupole.

that the peak to peak amplitude, $V_{CC,p-p}$, is the difference between the maximum positive and negative peaks of the signal. The uncertainty in the amplitude is defined as the offset that needs to be added or subtracted to the signal, such as it is centered around zero. In other words, the uncertainty, ΔV_{CC}, is defined as half the sum of the maximum positive and negative peaks of the signal. Figure 5.9 shows the peak to peak amplitude, $V_{CC,p-p}$, the amplitude of the signal, V_{CC}, and the uncertainty, ΔV_{CC}, for the reconstructed CC voltage, $V_{CC}(t)$.

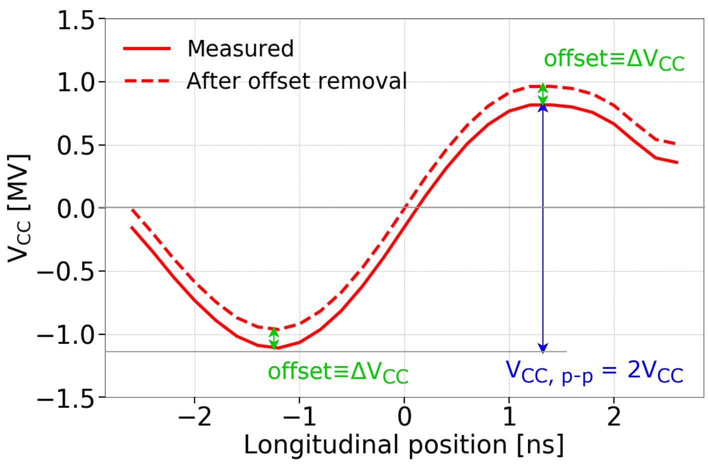

Figure 5.9: Illustration of the CC amplitude voltage, V_{CC}, defined as half the peak to peak amplitude, $V_{CC,p-p}$ (blue) and of its uncertainty, ΔV_{CC}, defined as the offset needed for the signal to be zero-centered. Here, V_{CC}=0.96 MV and ΔV_{CC}=0.15 MV.

Reconstruction of crabbing

Additionally, the measurements from the HT monitor were used for reconstructing the crabbing and representating schematically the beam projection in the transverse plane. The technique for reconstructing the crabbing was developed at CERN in 2018 and was extensively used throught the experimental campaign with CCs since (together with the calibrated voltage) it gives a straightforward estimate of the applied CC kick, as illustrated in Fig. 5.10.

To obtain this schematic representation, which is practically a density plot, of the effect of the CC kick on the beam one needs to multiply the measured longitudinal profile, mean of the sum signals acquired after the synchronisation, with the measured intra-bunch offset, mean of the differene signals acquired after the synchronisation. An example of this is shown in Fig. 5.7. For the transverse plane a gaussian distribution is considered with σ obtained from the wire scanner (addressed in more detail in the following section). The color code of Fig. 5.10 is normalised to the maximum intensity within the bunch.

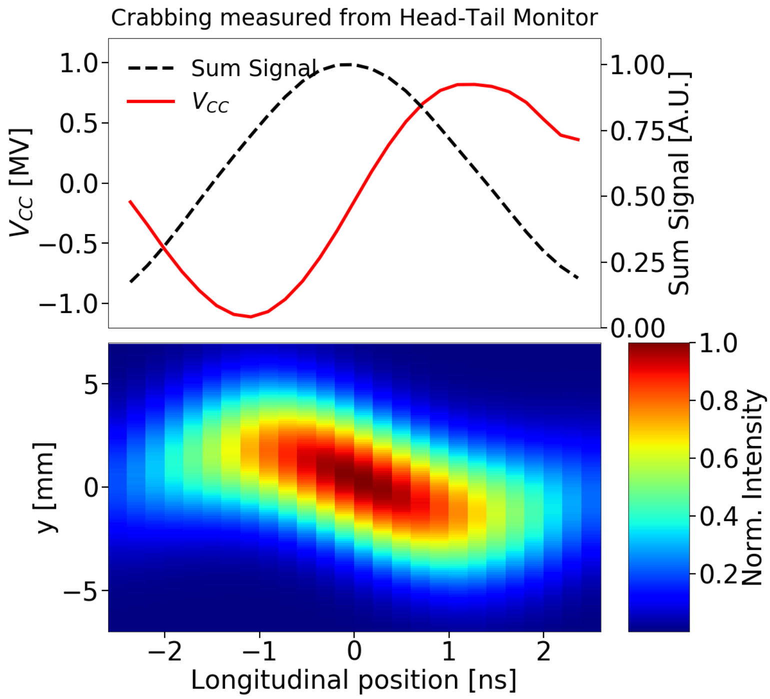

Figure 5.10: Illustration of the crabbing from the HT monitor signal. CC voltage and sum signal (longitudinal line density) measured from the HT monitor (top) together with the density plot (bottom) which visualises the effect of the CC kick in the beam.

5.4 SPS Wire Scanners

The SPS is equipped with Wire Scanners (WS) to measure the transverse beam emittance. The SPS WS system is described in detail in Ref. [19, 20]. For the SPS tests, the emittance was measured with WS both for the horizontal and vertical plane (BWS.51995.H and BWS.41677.V respectively).

The working principle is shown in Fig. 5.11. A thin wire rapidly moves across the proton beam and a shower of secondary particles is generated. The signal from the secondary particles is then detected by a system of scintillator and photomultiplier (PM) detectors outside of the beam pipe. By measuring the PM current as a function of wire position over multiple turns the transverse beam profile is reconstructed. An example of a vertical profile is shown in Fig. 5.12.

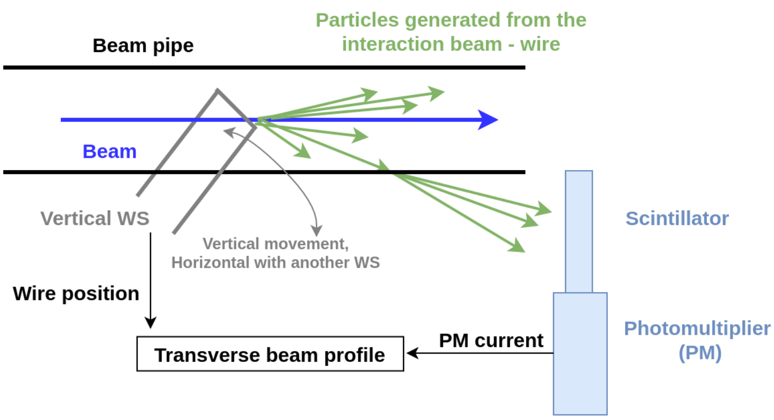

Figure 5.11: Sketch of the SPS rotational wire scanners [20]. The wire moves across the proton beam generating secondary particles which are then detecting by a scintillator and a photomultiplier. From the measured photomultiplier current the beam profile is reconstructed.

Fitting of transverse profiles

To obtain the beam size, σ, the standard procedure of fitting measured data to a model is followed [21]. In particular, the transverse profiles from each scan are fitted with the following four-parameter gaussian function:

$$f(x) = k + Ae^{-\frac{(x-\mu)^2}{2\sigma^2}}, \tag{5.2}$$

where k is the signal offset of the PM, A is the signal amplitude, μ is the mean of the

Gaussian distribution and σ its standard deviation. A non-linear least square minimization is used to fit the gaussian function to the measured data and obtain the optimal values for the parameters (A, k, μ, σ). The standard error of the parameters' estimates is given by the square root of the diagonal of their covariance matrix. [21]. The uncertainty of the measured beam size, $\Delta\sigma$, is defined as the standard error of the σ parameter. The optimal parameters' values and their covariance matrix are computed here using the scipy.curve_fit [22] function of Python programming language.

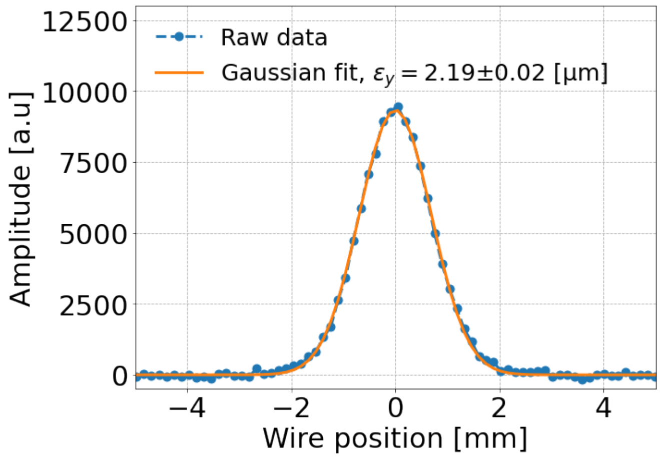

Figure 5.12: Vertical beam profile obtained from the BWS.41677.V instrument. The measured data points (light blue) are fitted with a four parameter Gaussian (orange) to obtain the beam size. The calculated emittance is also shown.

The general formula for computing the normalised beam emittance from the beam size, σ is given by:

$$\epsilon = \frac{\sigma^2}{\beta_{WS}}\beta\gamma, \tag{5.3}$$

where σ is the rms beam size, β_{WS} the beta function at the WS location and β, γ the relativistic parameters.

Note that, in the 2018 SPS operational configuration, the dispersion was small at the WSs location and thus its contribution to the beam size was considered to be negligible [1]. For the CC studies at 270 GeV beam energy, $\beta\gamma$ equals 287.8 and the beta

[1]The dispersion at BWS.51995.H location in 2018 was D_x= -15 mm. At 270 GeV, the energy spread, δ, is of the order of 10^{-4}. Thus, from Eq. (2.1) the horizontal normalised emittance from the dispersion is expected at the order of 10^{-6} μm. Comparing to the observed beam size during the CC tests

functions were 81.5 m and 62.96 m at the locations of the horizontal and vertical WS respectively. The uncertainty on the beta functions at the location of the WS, $\Delta\beta_{WS}$, is 5% in both planes, which represents the rms beta-beating in the SPS [23].

Assuming that the relativistic parameters are free of error, the uncertainty of the computed emittance, $\Delta\epsilon$, depends on the uncertainty of the measured beam size, $\Delta\sigma$ and of the beta function at the location of the WS, $\Delta\beta_{WS}$, as follows:

$$\Delta\epsilon = \sqrt{\left(\frac{\partial\epsilon}{\partial\sigma}\right)^2 \Delta\sigma^2 + \left(\frac{\partial\epsilon}{\partial\beta_{WS}}\right)^2 \Delta\beta_{WS}^2} = \epsilon\sqrt{\left(\frac{2\Delta\sigma}{\sigma}\right)^2 + \left(\frac{\Delta\beta_{WS}}{\beta_{WS}}\right)^2}. \tag{5.4}$$

Further considerations

It is worth noting here that during each measurement with the WS the beam profile is actually acquired twice as the wire crosses the beam in the forward direction (IN scan) and then in the reverse direction (OUT scan). For the 2018 measurements the emittance values obtained from IN and OUT scans, $\epsilon_{\mathrm{IN}} \pm \Delta\epsilon_{\mathrm{IN}}$ and $\epsilon_{\mathrm{OUT}} \pm \Delta\epsilon_{\mathrm{OUT}}$, were found to be very similar. In the analysis of the 2018 measurements, the average emittance from the two scans, $\epsilon_{\mathrm{avg}} = \langle\epsilon_{\mathrm{IN}}, \epsilon_{\mathrm{OUT}}\rangle$, is used. The uncertainty in the average, $\Delta\epsilon_{\mathrm{avg},1}$, is given by (see Appendix ...):

$$\Delta\epsilon_{\mathrm{avg},1} = \frac{|\,\epsilon_{\mathrm{IN}} - \epsilon_{\mathrm{OUT}}\,|}{2\sqrt{2}}. \tag{5.5}$$

The propagated uncertainty from the measurement errors, $\Delta\epsilon_{\mathrm{IN}}$ and $\Delta\epsilon_{\mathrm{OUT}}$, is given by:

$$\Delta\epsilon_{\mathrm{avg},2} = \frac{1}{2}\sqrt{\Delta\epsilon_{\mathrm{IN}}^2 + \Delta\epsilon_{\mathrm{OUT}}^2}. \tag{5.6}$$

Considering that $\Delta\epsilon_{\mathrm{avg},1}$ and $\Delta\epsilon_{\mathrm{avg},2}$ are independent, the combined uncertainty in the average, $\Delta\epsilon_{\mathrm{avg}}$, is given by:

$$\Delta\epsilon_{\mathrm{avg}} = \sqrt{\Delta\epsilon_{\mathrm{avg},1}^2 + \Delta\epsilon_{\mathrm{avg},2}^2}. \tag{5.7}$$

Finally, some emittance increase is expected during each wire scan, due to multiple Coulomb scattering. This effect has been extensively studied in Ref. [24]. For the

of a few microns the dispersion is negligible. The measured D_x, D_y were found to be very small and thus their contribution is also considered negligible. The plan is to perform some measurments in 2022 to get a feeling of their values at the location of the wire scanners rotational SPS WS and the energy of 270 GeV, at which the CC experiments were performed the expected emittance growth from the WS is expected to be small. However, a conservative number of scans were carried, ~ 20 scans per bunch and per plane during ~ 1 hour, in order to minimise the contribution from this effect.

5.5 ABWLM and Wall Current monitor

The bunch length was measured with two different instruments the ABWLM (A for RF, Beam, Wideband, Longitudinal, Measurement) [25] and the Wall Current monitor [26]. The ABWLM measures the longitudinal profiles from which the bunch length is computed by performing a gaussian fit. The Wall Current monitor acquirest not just the longitudinal profiles but also the longitudinal beam position relative to the monitor i.e. the beam arrival with respect to the reference. The bunch length is estimated by computing the full width half maximum of the profiles and then using it to estimate the sigma of a gaussian distribution. No further details on the operation of these instruments are discussed here as the offline analysis was not performed by the author.

6 | Experimental studies 2018: Measurements and analysis

In Chapter 5 the operational set up and the beam instrumentation used for the first measurements of noise induced emittance growth with CC and proton beams in the SPS were described.

In this Chapter the experimental results are discussed. In particular, the measurements of the paramters of interest (described in Chapter 3, Eq. (3.1) and Eq. (3.2)) and their analysis are presented. First, Section 6.1 explains the experimental procedure. In Section 6.2 the calibration of the CC voltage is displayed. Section 6.3 elaborates on the injected noise and the acquistions of the power spectrum. Thereafter, in Section 6.4 the measured emittance growth, which is the paramter of primary interest, is discussed. Furthermore, the measurements of the bunch length are examined in Section 6.5 while the intensity evolution is shown in Section 6.6 for completness. Section 6.7 compares the measured emittance growth rates with the predictions of the theoretical model introduced in Chapter 3. Finally, Section 6.8 summarizes the main experimental findings.

6.1 Experimental procedure

The dedicated experiment to study the emittance growth induced by noise in the CC RF sytsem took place on September 5, 2018, and was given a total time window of about 16 hours (start:~10:30, end:~17:00). Remember that the goal was to benchmark the analytical model (see Chapter 3) with experimental data.

The beam and machine conditions for the emittance growth studies were discussed extensively in Chapter 5 and are listed in Tables 5.1 and 4.1. To summarise, the measurements were performed with four bunches, seperated by 524 ns, at 270 GeV with low intensity (3×10^{10} ppb) and with linear chromaticity corrected to ~ 1. The Landau octupoles and the transverse feedback system were switched off. Only CC2 was used, with voltage of ~1 MV, providing a vertical kick on the beam. That configuration remained unchanged during the experiment.

In order to characterize the CC noise induced emittance growth, different levels of controlled noise were injected into its LLRF system and the bunch evolution was recorded for about 20-40 minutes (for each noise setting). The experiment was conducted over three "coasts", sinnce a new beam was injected every time the quality of the beam was seen to be degraded e.g. very large beam size.

6.2 Crab cavity voltage. Change beta functions of CC at the scripts, and the pay –> phase advance!!!

As already mentioned above, the targetd CC voltage was 1 MV. Nevetherless, beam based measurements with the HT monitor (post-processing in Section 5.3) were carried out to validate this value. Unfortunately, only two measurements are available, which are displayed in Fig. 6.1. The first measurement took place before the start of the first "coast", at ~9:45 (left), while the second one took place at ~13:50 between the first and the seond "coast" (right).

The amplitude of the CC voltage was measured to be 0.75 ± 0.37 MV and 0.96 ± 0.04 MV from the first and the second acquisition respectively. In the following analysis the averaged CC voltage from the two scans, $V_{CC,\mathrm{avg}} = 0.86 \pm 0.2$ MV , will be used. The uncertainty $\Delta V_{CC,\mathrm{avg}} = 0.2$ MV .. is computed as follows.

First, the uncertainty in the average, $\Delta V_{CC,\mathrm{avg1}}$, is estimated by (see Appendix ...):

$$\Delta V_{CC,\mathrm{avg1}} = \frac{|\,0.75 - 0.96\,|}{2\sqrt{2}} = 0.074 \text{ MV}. \tag{6.1}$$

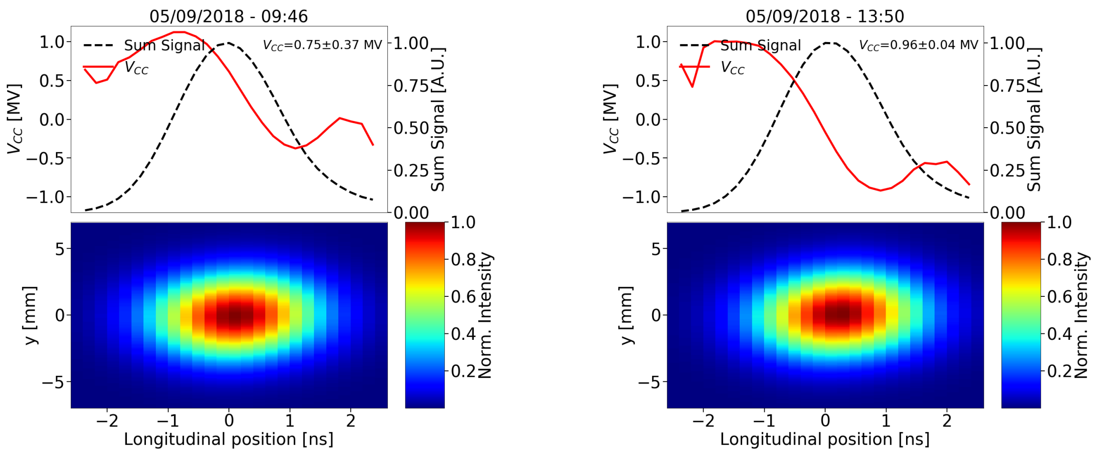

Figure 6.1: Measurements of the CC voltage, with the HT monitor (see Section 5.3.1), before(top-left) and during (top-right) the emittance growth studies. The density plots (bottom) are also shown here to point out that the crabbing is not clearly visible at the energy of 270 GeV, especially compared to the studies at lower energy (Fig. 5.10).

Then the propagated uncertainty from the measurement errors, 0.37 MV and 0.04 MV, is estimated by:

$$\Delta V_{CC,\mathrm{avg2}} = \frac{1}{2}\sqrt{0.37^2 + 0.04^2} = 0.19\ \mathrm{MV}. \tag{6.2}$$

Considering that $\Delta V_{CC,\mathrm{avg1}}$ and $\Delta V_{CC,\mathrm{avg2}}$ are independent, the combined uncertainty in the average, $\Delta V_{CC,\mathrm{avg}}$, is given by:

$$\Delta V_{CC,\mathrm{avg}} = \sqrt{\Delta V^2_{CC,\mathrm{avg1}} + \Delta V^2_{CC,\mathrm{avg2}}} = 0.2\ \mathrm{MV}. \tag{6.3}$$

6.3 Injected RF noise

The injected RF noise was a mixture of amplitude and phase noise up to 10 kHz, overlapping and primarily exciting the first betatron sideband at ~ 8 kHz. The phase noise was always dominant. Figure 6.2 dsiplays two example measurements of phase (left) and amplitude (right) noise acquired during the experiment with a sepctrum analyzer E5052B [27].

The following needs to be refined. I struggled to write it.

Emittance growth measurements were performed for seven different noise levels,

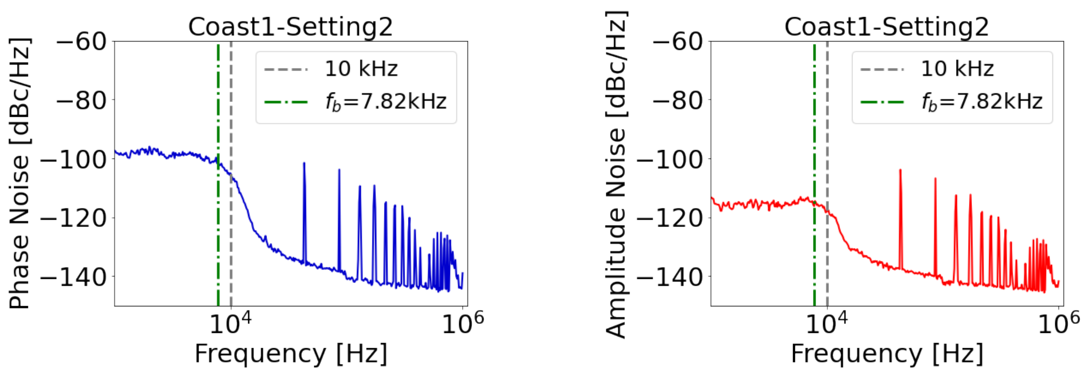

Figure 6.2: Example phase (left) and amplitude (right) noise spectra measured with a spectrum analyzer E5052B during the emittance growth studies with CCs in SPS. The noise spread-out up to 10 kHz (grey dashed line) exciting the first betatron sideband at ~8 kHz (green dashed line). The spikes at high frequencies correspond to the harmonics of the revolution frequency and are a result of the bunch crossing.

listed in Table 6.1. The following two points should be highlighted regarding its listings.

- As already discussed in Chapter 3 the noise induced emittance growth depends on the noise power at the beteatron and synchrobetatron sidebands for the phase and amplitude noise respectively (see Eq. 3.2 and Eq. 3.1). Therefore, the noise power values of interest for this thesis are the ones at the first betatron $f_b = 0.18 \times f_{rev} = 7.82$ kHz and at the synchrobetatron sidebands at $f_b \pm \mathrm{Q_s} \times f_{rev} = f_b \pm \sim 220$ kHz. In the following, it is assumed for simplicity that the noise power at the sidebands mentioned above is the same. Here this assumption is acceptable since the noise power in the measurements is basically constant for all frequencies up to 10 KHz.

- It is clear from Fig. 6.2 that the measurements are noisy. In particular random changes in amplitude are observed from point to point within the signal. The values listed in Table 6.1 correspond to the averaged noise values over a frequency range of $\pm$ 500 Hz around the betatron frequency. The unceratinties show the spread of the values and are defined

This spectrum analyzer provides a single sideband measurement (SSB), which is expressed as $10\log_{10}\mathscr{L}(f)$ [dBc/Hz]. Its relation with the power spectral densities

Table 6.1: Phase and amplitude noise levels injected in the CC RF system for the emittance growth studies in 2018.

	$\mathbf{10\log_{10}\mathscr{L}(f)}$ **[dBc/Hz]**	
	Phase noise	**Amplitude noise**
Coast1-Setting1	-122.6 ±0.6	-128.1 ± 0.6
Coast1-Setting2	-101.4 ± 0.8	-115.2 ± 0.6
Coast2-Setting1	-115.1 ± 0.8	-124.1 ± 0.5
Coast2-Setting2	-111.4 ± 0.6	-115.7 ± 0.4
Coast3-Setting1	-110.9 ± 0.9	-116.9 ± 0.4
Coast3-Setting2	-106.4 ± 0.3	-112.9 ± 0.6
Coast3-Setting3	-101.4 ± 0.7	-106.9 ± 0.5

(PSDs) introduced in Eq. (3.1) and Eq. (3.2) are given by $S_\Delta = 2\mathscr{L}(f)$ [28], with $S_{\Delta A}$ in 1/Hz and $S_{\Delta\phi}$ in rad^2/Hz. A detailed discussion on the noise power measurements and their relation to the mathimatical defintion of the PSD is given in Chapter [tba].

As already mentioned above, the injected noise was a combination of both phase and amplitude noise. Therefore, in order to make a meaningful comparison between the different noise levels the concept of effective phase noise is introduced. This is the phase noise level that would lead to the same emittance growth as that from both phase and amplitude noise. The noise levels mentioned in this chapter correspond to the calculated effective phase noise.

6.4 Emittance growth measurements

An overview of the bunch by bunch emittance growth measurments is shown in Fig ... for both horizontal (top) and vertical (bottom) plane. The four different colors (blue, orange, green, red) correspond to the four different bunches. The three "coasts" are distinguishable with the black dashed vertical lines. For each "coast" a new beam was injected with the same targeted initial conditions. The different levels of injected noise are also displayed in the plot (bottom) while the moments at which the noise level changed are shown with the grey dashed vertical lines. These noise levels are the average of the effective phase noise over the four bunches (due to different bunch lengths.)

What should be observed is the following: ...

MD emittance growth overview. - average from IN and OUT. As mentioned in CH4. vs time and vs noise level for all bunches. Not yet comparison with the theory. Probably you need to re-run this to make correctly the error propagation. - 1 noise point was excluded

6.5 Bunch length measurements

- bunch length and longitudinal profiles and relative position from the wall current monitor. unstable bunches. - bunch 2-3-4 longutidinally unstable.

6.6 Intensity measurements

No losses. Maybe not seperate chapter? I should also mention in Ch4 how the emittance is measured from the ABWLM.

6.7 Comparison of measured emittance growth with the theory

Comparison of bunch 1 with theory. Discrepancy of a factor 4.

6.8 Conclusions and outlook

test line for new branch.

7 Investigation of the discrepancy

7.1 Sensitvity studies

1. Sensitvity to how noisy is the noise spectrum 2. On the CC voltage 3. On the different bunch lengths.

7.2 b3b5b7 multiple errors

Contribution of the non-linearities with sixtracklib.

8 | Simple model of describing the decoherence suppression from impedance

9 | Application and impact for HL-LHC

10 | Conclusion

A | Appendix Title

For the uncertainty in the mean: https://www.physics.upenn.edu/sites/default/files/Managing

B | Glossary

Peak to peak: Peak-to-peak (pk-pk) is the difference between the maximum positive and the maximum negative amplitudes of the wave.

https://electronics.stackexchange.com/questions/313269/peak-to-peak-vs-amplitude

Landau octupoles

Bibliography

[1] *Official optics repository of the CERN Super Proton Synchrotron (official name SPS)*. Accessed: 16-2-2022. URL: https://gitlab.cern.ch/acc-models/acc-models-sps/-/tree/2021/.

[2] P. Baudrenghien and T. Mastoridis. “Transverse emittance growth due to rf noise in the high-luminosity LHC crab cavities”. In: *Phys. Rev. ST Accel. Beams* 18 (10 Oct. 2015), p. 101001. DOI: 10.1103/PhysRevSTAB.18.101001. URL: https://link.aps.org/doi/10.1103/PhysRevSTAB.18.101001.

[3] A. Papoulis. *Probability, Random Variables, and Stochastic Processes.* Communications and Signal Processing. McGraw-Hill, 1991. ISBN: 9780070484771. URL: https://books.google.ch/books?id=4IwQAQAAIAAJ.

[4] C. Zanoni et al. “The crab cavities cryomodule for SPS test”. In: 874 (July 2017), p. 012092. DOI: 10.1088/1742-6596/874/1/012092. URL: https://doi.org/10.1088/1742-6596/874/1/012092.

[5] Rama Calaga, Ofelia Capatina, and Giovanna Vandoni. “The SPS Tests of the HL-LHC Crab Cavities”. In: (2018), TUPAF057. 4 p. DOI: 10.18429/JACoW-IPAC2018-TUPAF057. URL: https://cds.cern.ch/record/2649807.

[6] P Baudrenghien et al. “Functional Specifications of the LHC Prototype Crab Cavity System”. In: (Feb. 2013). URL: https://cds.cern.ch/record/1520896.

[7] Rama Calaga. *SPS Crab Cavity test RF Test Program.* Accessed: 11-11-2021. URL: https://indico.cern.ch/event/718127/contributions/2951305/attachments/1645650/2629988/SPSCCtestv3.pdf.

[8] Carver Lee. *First proton beam dynamics results with crab cavities*. Accessed: 10-11-2021. URL: https://indico.cern.ch/event/800428/attachments/1804664/2945632/CrabCavity_BE_Seminar.pdf.

[9] R. Jones and H. Schmickler. "The measurement of Q' and Q" in the CERN-SPS by head-tail phase shift analysis". In: *PACS2001. Proceedings of the 2001 Particle Accelerator Conference (Cat. No.01CH37268)*. Vol. 1. 2001, 531–533 vol.1. DOI: 10.1109/PAC.2001.987561.

[10] Thomas Levens, Kacper Łasocha, and Thibaut Lefèvre. "Recent Developments for Instability Monitoring at the LHC". In: (2017), THAL02. 4 p. DOI: 10.18429/JACoW-IBIC2016-THAL02. URL: https://cds.cern.ch/record/2313358.

[11] T. E. Levens et al. "Automatic detection of transverse beam instabilities in the Large Hadron Collider". In: *Phys. Rev. Accel. Beams* 22 (11 Nov. 2019), p. 112803. DOI: 10.1103/PhysRevAccelBeams.22.112803. URL: https://link.aps.org/doi/10.1103/PhysRevAccelBeams.22.112803.

[12] Tom Levens. *Beam instrumentation with SPS Crabs*. Accessed: 11-11-2021. URL: https://indico.cern.ch/event/718127/contributions/2951309/attachments/1646050/2630808/BI_SPS_Crabs.pdf.

[13] Alexander Wu Chao et al. *Handbook of accelerator physics and engineering; 2nd ed.* Singapore: World Scientific, 2013. DOI: 10.1142/8543. URL: https://cds.cern.ch/record/1490001.

[14] R Calaga et al. "Proton-beam emittance growth in SPS coasts". In: *Conf. Proc.* C1205201 (May 2012), THPPP007. 3 p. URL: https://cds.cern.ch/record/1451286.

[15] A Alekou et al. *Emittance growth in coast in the SPS*. Accessed: 26-11-2021. URL: https://indico.cern.ch/event/609486/contributions/2457542/attachments/1433340/2318716/EmittanceEvolutionCoastSPS_2017_April.pdf.

[16] Fanouria Antoniou et al. "Emittance Growth in Coast in the SPS at CERN". In: *J. Phys.: Conf. Ser.* 1067 (2018), MOPMF061. 7 p. DOI: 10.18429/JACoW-IPAC2018-MOPMF061. URL: https://cds.cern.ch/record/2649815.

[17] Michele Carlà et al. "Studies of a New Optics With Intermediate Transition Energy as Alternative for High Intensity LHC Beams in the CERN SPS". In: (2018), TUPAF022. 4 p. DOI: 10.18429/JACoW-IPAC2018-TUPAF022. URL: https://cds.cern.ch/record/2664976.

[18] Androula Alekou et al. "SPS Long Term Stability Studies in the Presence of Crab Cavities and High Order Multipoles". In: (2018), WEP2PO008. 3 p. DOI: 10.18429/JACoW-HB2018-WEP2PO008. URL: https://cds.cern.ch/record/2640326.

[19] J. Bosser et al. "Transverse emittance measurement with a rapid wire scanner at the CERN SPS". In: *Nuclear Instruments and Methods in Physics Research Section A: Accelerators, Spectrometers, Detectors and Associated Equipment* 235.3 (1985), pp. 475–480. ISSN: 0168-9002. DOI: https://doi.org/10.1016/0168-9002(85)90096-8. URL: https://www.sciencedirect.com/science/article/pii/0168900285900968.

[20] OE Berrig et al. *CERN-SPS Wire Scanner Impedance and Wire Heating Studies*. Tech. rep. Geneva: CERN, Sept. 2014. URL: https://cds.cern.ch/record/1972478.

[21] Henri P. Gavin. *Fitting Models to Data, Generalized Linear Least Squares, and Error Analysis*. Accessed: 16-2-2022. URL: https://people.duke.edu/~hpgavin/SystemID/CourseNotes/linear-least-squres.pdf.

[22] *SciPy API Documentation*. Accessed: 16-2-2022. URL: https://docs.scipy.org/doc/scipy/reference/generated/scipy.optimize.curve_fit.html.

[23] Rogelio Tomas et al. "Improved algorithms to determine the non-linear optics model of the SPS from non-linear chromaticity". In: July 2007, pp. 4231–4233. ISBN: 978-1-4244-0916-7. DOI: 10.1109/PAC.2007.4439986.

[24] Federico Roncarolo. "Accuracy of the Transverse Emittance Measurements of the CERN Large Hadron Collider". Presented 2005. 2005. URL: https://cds.cern.ch/record/1481835.

[25] F. Follin G. Papotti. *Online bunch length measurement for SPS OP*. Accessed: 26-11-2021. URL: https://indico.cern.ch/event/774525/contributions/3218683/attachments/1756129/2847423/20181120_LIUSPSBD.pdf.

[26] G Papotti. “A Beam Quality Monitor for LHC Beams in the SPS”. In: (Sept. 2008), 4 p. URL: https://cds.cern.ch/record/1124099.

[27] K. Gheen. *Phase Noise Measurement Methods and Techniques.* Accessed November 5, 2020. Agilent Technologies. URL: https://studylib.net/doc/18034081/phase-noise-measurements.

[28] “IEEE Standard Definitions of Physical Quantities for Fundamental Frequency and Time Metrology—Random Instabilities”. In: *IEEE Std Std 1139-2008* (2009), pp. c1–35. DOI: 10.1109/IEEESTD.2008.4797525.